Special Problems in the Estimation of Power-Law Spectra as Applied to Topographical Modeling

Richard T. Austin, *Student Member, IEEE,* Anthony W. England, *Senior Member, IEEE,* and Gregory H. Wakefield, *Member, IEEE*

***Abstract*—An increasing number of topographical studies find that natural surfaces possess power-law roughness spectra. Power-law spectra introduce unique difficulties in the spectral estimation process. We describe how an improper window choice allows leakage that yields a spectral estimate that is insensitive to the spectral slope. In addition, the commonly used Fourier-based spectral estimates have higher variances than other available estimators. Higher variance is particularly problematic when data records are short, as is often the case in remote-sensing studies. We show that Capon's spectral estimator has less variance than Fourier-based estimators and measures the spectral slope more accurately. We also show how estimates of a 2-D roughness spectrum can be obtained from estimates of the 1-D spectrum for the isotropic power-law case.**

I. Introduction

SPECTRAL analysis is a tool of increasing importance in the characterization of natural surfaces. One- and two-dimensional spectral estimates are useful because they allow surface structure to be interpreted as a sum of sinusoidal components with differing wavelengths. A number of studies have found that spectra computed from one-dimensional surface profiles may be reasonably modeled using a power-law spectrum of the form

$$S_Z(f) = c\,|f|^{-\beta} \tag{1}$$

over some range of spatial frequencies. $S_Z(f)$ is the power spectral density of the surface height random process; it has units of meters^2/meters^{-1} or meters^2 per unit spatial frequency. The spectral exponent β indicates the relative contribution of different wavelength components. Higher values of β indicate that the surface roughness is mostly due to low-frequency components, while lower values denote significant high-frequency contributions. β is also known as the spectral slope; a power-law spectrum is linear with slope $-\beta$ when plotted on a log–log scale. The roughness amplitude c is a multiplicative factor scaling the roughness at all spatial frequencies. Applications of power-law spectra include studies of regional topography [1]–[5], rock surfaces [6], seafloor morphology [7]–[11], and other surfaces [12], [13].

Rough surfaces that have structure over a wide range of spatial scales may also be described using the concepts of fractal geometry introduced by Mandelbrot [14]. Fractal objects are continuous but not differentiable; the fractal dimension D_f is a real-valued measure of how a line (surface) fills a plane (space). For a one-dimensional (1-D) surface profile, D_f takes on values between 1.0 (smooth and differentiable) and 2.0 (plane-filling). Two-dimensional (2-D) surfaces have D_f between 2.0 and 3.0. Adler [15] shows that the surface profile created by the intersection of a plane and a 2-D fractal surface is itself fractal with a fractal dimension equal to that of the 2-D surface decreased by one [2]. Random rough fractal surfaces have power-law spectra; Mandelbrot and Van Ness [16] and Voss [17] derive the relation between D_f and the spectral slope β of a 1-D profile of a rough fractal surface:

$$D_f = \frac{5 - \beta}{2}. \tag{2}$$

Thus, the spectral exponent satisfies $3 > \beta > 1$ for $1 < D_f < 2$.

Although synthetic topographies appear most realistic with $D_f \approx 2.2$ [14], [17], yielding linear profiles of $D_f \approx 1.2$ and $\beta \approx 2.6$, several studies [1], [4], [7], [8] have reported measured values of $\hat{\beta}$ (the hat denotes an estimate) near 2.0, leading some investigators to suggest that spectral slopes of 2.0 are characteristic of natural topography [1]. One explanation for the discrepancy between measured $\hat{\beta}$ and inferred values of β is that spectral analysis of nonstationary regions tends to result in $\hat{\beta}$ near 2.0 [9], [18]. We show in this paper that leakage in spectral estimators may also yield $\hat{\beta}$ that cluster near 2.0.

While leakage is a well-known problem of classical spectral estimators such as the periodogram, common Fourier-based spectral estimators also suffer from high variance. The usual remedy is to average spectral estimates derived from multiple data sets or multiple segments of a long data set. This is not always possible: in remote-sensing studies, surface profiles are often only one of many "ground-truth" parameters to be collected. As a result, investigators may be faced with the problem of estimating the surface spectrum using a limited data set.[1] In

Manuscript received May 29, 1993; revised March 18, 1994. This work was supported in part by the National Aeronautics and Space Administration under Grant NAGW-2199 and by a shared SIR-C project.

The authors are with the Department of Electrical Engineering and Computer Science, University of Michigan, Ann Arbor, MI 48109.

IEEE Log Number 9402672.

[1] In the case of 1-D surface profiles, we find that a typical record consists of at most 500 points; 2-D profiles are even shorter, rarely exceeding 50 × 50 points. Numbers of this magnitude are considered small from a statistical inference viewpoint, where samples of thousands or hundreds of thousands of points are more common.

this paper, we describe a spectral estimator that reduces the leakage problem and predicts c and β with reduced variance in the case of short data runs.

II. Spectral Estimates from Linear Profiles

Fourier-based spectral estimators (e.g., the periodogram) render an estimate of the power spectral density whose expectation or mean value is a convolution of the spectrum of the sampled profile and the Fourier transform of a window function introduced by the finite extent of the sample profile. Various window functions are used; common windows include rectangular, triangular, and Hanning windows. The selection of a particular window is based on a trade-off between spectral resolution and spectral leakage.

Spectral leakage refers to the inaccuracy of a spectral estimate at a given frequency due to convolution with the transformed window; i.e., spectral power "leaks" from nearby frequencies according to the shape of the transformed window. We show spectral domain window functions corresponding to a periodogram and a modified periodogram with Hanning window in Fig. 1. At each point or frequency at which the spectrum is to be estimated, the true spectrum (the dashed line in Fig. 1) is weighted by the window function centered on that frequency and then averaged over frequency. Contributions from frequencies other than the frequency of interest constitute spectral leakage. We can reduce spectral leakage by choosing an estimator whose window has sidelobes that decay quickly (such as W_H in Fig. 1), but such a window will have a broader main lobe, decreasing the spectral resolution. (See [19] for a discussion.) In the power-law case, leakage from the large peak at low spatial frequencies affects the estimate at upper spatial frequencies (making the slope shallower) unless a window function with very low sidelobe levels is selected. We now show this result for the case of 1-D spectral estimates based on 1-D surface profiles.

Spectral estimates derived from sampled data suffer from *aliasing* if the sampled process has spectral components at frequencies greater than the Nyquist frequency f_c,

$$f_c = \frac{1}{2\Delta} \tag{3}$$

where Δ is the sampling interval. In the sections that follow, we will assume that aliasing is not present. Simulated data sets will be bandlimited to prevent aliasing. Modifications due to aliasing will be presented in a later section.

A. Fourier-Based Estimators

Consider a one-dimensional surface $Z(x)$, where Z, the surface height, is a single-valued function (i.e., there are no overhangs). Suppose that the surface height has been measured at N locations x_i ($i = 0, \cdots, N-1$), which

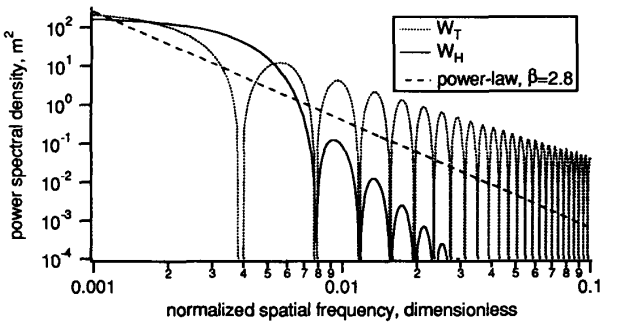

Fig. 1. Spectral domain window functions W_T (10) for the periodogram and W_H (13) for the modified periodogram with Hanning window, both with $N = 256$. The convolution of the window function with the true spectrum (e.g., the power-law spectrum shown as the dashed line) may result in a spectral bias (an inaccuracy in the mean value of the estimate).

are spaced at intervals Δ. The periodogram spectral estimator $\hat{P}_{\mathrm{PER}}(f_\Delta)$ for the sampled surface height is given by Kay [20]:

$$\hat{P}_{\mathrm{PER}}(f_\Delta) = \frac{1}{N}\left|\sum_{n=0}^{N-1} Z[x_n] \exp\left(-j2\pi f_\Delta n\right)\right|^2. \tag{4}$$

The frequency is written f_Δ as a reminder that (4) is given in terms of a normalized frequency f_Δ, where

$$f_\Delta = f\Delta \tag{5}$$

and f_Δ satisfies $-\frac{1}{2} \le f_\Delta \le \frac{1}{2}$. (Most spectral estimation texts use normalized frequency; we will follow this convention until a later section when we compare spectra obtained from sampled profiles with differing Δ.)

While the periodogram may be evaluated for any $|f_\Delta|$ less than $\frac{1}{2}$ (the normalized Nyquist frequency), it is often calculated using a fast Fourier transform (FFT) and consequently is evaluated only at discrete frequencies $f_{\Delta i} = i/N$, where $i = -N/2, \cdots, -1, 0, 1, \cdots, N/2$. To evaluate the periodogram using an FFT at additional frequencies, we can "zero-pad" the original data series to length M by adding $M - N$ zeros to the end. The periodogram will then be evaluated at frequencies $f_{\Delta i} = i/M$. Most FFT algorithms require that N be an integer power of two. Series for which N is not an integer power of two must be zero-padded up to the next higher power of two.

The periodogram is an unreliable estimator of the power spectral density because it has a variance that is equal to the square of its expected value, *independent of* N [20]. The usual practice in the field of spectral estimation is to average multiple periodograms to reduce the variance, but this may not be possible if the quantity of data is limited.[2] We show later in this section that $\hat{P}_{\mathrm{PER}}$ is a poor estimator in the power-law case even if the variance problem were absent.

[2]For example, suppose the data record is 1000 points long. To reduce the variance by a factor of eight, we can divide the data record into eight segments of length 125, calculate eight spectral estimates, and average the results. The bias of the estimate will be increased (due to the broader main and side lobes of the window), and the reduction in variance may be less than eightfold if the segments are not uncorrelated. If the entire data record has only 125 points, this procedure is not useful.

A modified periodogram $\hat{P}_{\mathrm{HAN}}(f_\Delta)$ may be obtained by multiplying the data series by a Hanning window before calculating the spectral estimate:

$$\hat{P}_{\mathrm{HAN}}(f_\Delta) = \frac{1}{NU}\left|\sum_{n=0}^{N-1} Z[x_n]\, w_H[n] \exp\left(-j2\pi f_\Delta n\right)\right|^2 \quad (6)$$

where the Hanning window

$$w_H[n] = \frac{1}{2}\left[1 - \cos\left(\frac{2\pi n}{N-1}\right)\right] \quad (7)$$

replaces the rectangular window ($w_R[n] = 1$) implicit in (4), and an extra normalization factor is introduced:

$$U = \frac{1}{N}\sum_{n=0}^{N-1} w_H^2[n]. \quad (8)$$

(Equation (6) follows the formulation of Welch [21] using a single data segment.) The transform of the Hanning window $w_H[n]$ has sidelobes that are lower and a main lobe that is roughly twice as wide as that of the transform of a rectangular window $w_R[n]$ of the same width. Convolution with a transformed Hanning window results in less leakage from low spatial frequencies (because the sidelobes are smaller) at the cost of decreased spectral resolution (smoothing due to the wider main lobe). We must consider the smoothness of the spectrum and how quickly it rolls off and then decide whether the leakage reduction is worth the loss in resolution. In the power-law case, reducing the leakage seems more important.

We now examine the expected values of these two estimators for a power-law surface spectrum. The expectation of the periodogram is given by [20]

$$E[\hat{P}_{\mathrm{PER}}(f_\Delta)] = \int_{-1/2}^{1/2} W_T(f_\Delta - \xi)\, S_{Z\Delta}(\xi)\, d\xi \quad (9)$$

where $W_T(f_\Delta)$ is the transform of a triangular window:

$$W_T(f_\Delta) = \frac{1}{N}\left(\frac{\sin \pi f_\Delta N}{\sin \pi f_\Delta}\right)^2 \quad (10)$$

and $S_{Z\Delta}(f_\Delta)$ is the normalized form of the true power spectral density of $Z(x)$ chosen such that $\int S_{Z\Delta}(f_\Delta)\, df_\Delta = \int S_Z(f)\, df$:

$$\begin{aligned} S_{Z\Delta}(f\Delta) &= \frac{1}{\Delta} S_Z(f) \\ &= \frac{1}{\Delta} c f^{-\beta} \\ &= \Delta^{\beta-1} c (f\Delta)^{-\beta} \\ S_{Z\Delta}(f_\Delta) &= c_\Delta f_\Delta^{-\beta}. \end{aligned} \quad (11)$$

The expected value of the modified periodogram estimator $\hat{P}_{\mathrm{HAN}}$ has a form similar to (9) [23, p. 553]:

$$E[\hat{P}_{\mathrm{HAN}}(f_\Delta)] = \int_{-1/2}^{1/2} W_H(f_\Delta - \xi)\, S_{Z\Delta}(\xi)\, d\xi \quad (12)$$

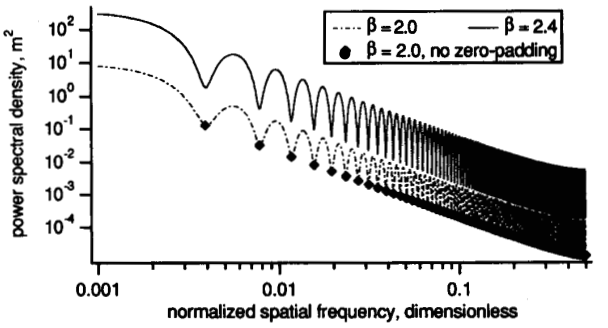

Fig. 2. Expected value of the periodogram spectral estimator for power-law surfaces with $\beta = 2.0$ and 2.4 and $c_\Delta = 1.0 \cdot 10^{-6}$. The estimates are based on 256-point profiles that were zero-padded to 16 384 points so that the periodogram would be evaluated at many frequencies. Solid dots indicate the expected values of the periodogram when evaluated without zero-padding.

where

$$W_H(f_\Delta) = \frac{1}{4NU}\left(b_1 + \frac{1}{2}b_2 + \frac{1}{2}b_3\right)^2 \quad (13)$$

$$b_1 = \frac{\sin(\pi f_\Delta N)}{\sin(\pi f_\Delta)} \quad (14)$$

$$b_2 = \frac{\sin\left\{\pi\left[f_\Delta - \frac{1}{N-1}\right]N\right\}}{\sin\left\{\pi\left[f_\Delta - \frac{1}{N-1}\right]\right\}} \quad (15)$$

$$b_3 = \frac{\sin\left\{\pi\left[f_\Delta + \frac{1}{N-1}\right]N\right\}}{\sin\left\{\pi\left[f_\Delta + \frac{1}{N-1}\right]\right\}} \quad (16)$$

and U is given by (8).

To show the performance of these Fourier-based estimators, we calculate their expected values using (9) and (12). We avoid the singularity at the low end of a pure power-law spectrum by modeling the exact surface spectrum as a Rayleigh function at low spatial frequencies:

$$S_{Z\Delta}(f_\Delta) = \begin{cases} (\alpha/\sigma^2)\,|f_\Delta| \exp\left(-f_\Delta^2/[2\sigma^2]\right), \\ \qquad |f_\Delta| \le 0.0001 \\ c_\Delta |f_\Delta|^{-\beta} \\ \qquad 0.0001 \le |f_\Delta| \le \frac{1}{2} \\ 0, \quad |f_\Delta| > \frac{1}{2} \end{cases} \quad (17)$$

where the parameters α and σ are chosen by enforcing the continuity of $S_{Z\Delta}$ and its first derivative at $|f_\Delta| = 0.0001$.

Fig. 2 shows the expected value of the periodogram spectral estimator calculated from theoretical spectra with spectral exponents of 2.0 and 2.4. The oscillatory behavior is due to the sidelobes of $W_T(f_\Delta)$. These oscillations are not visible if the periodogram is evaluated only at frequencies $f_i = i/N$ (i.e., without zero-padding) as indicated

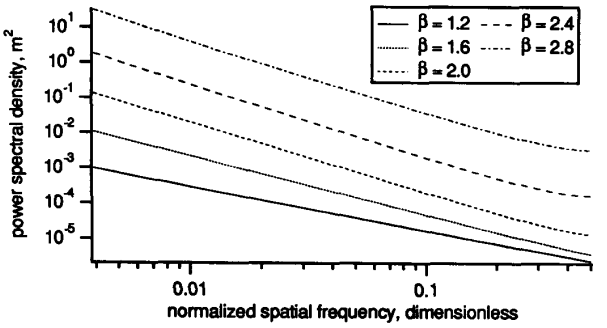

Fig. 3. Expected value of $\hat{P}_{PER}$ for five 256-point power-law profiles evaluated at frequencies corresponding to the case of no zero-padding.

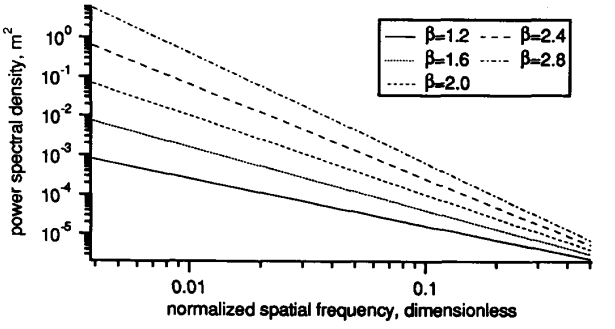

Fig. 4. Exact values of the power-law spectra used in calculations of the expected values of the spectral estimates.

in the figure. Since it is difficult to fit power-law functions to such oscillatory estimates, we sampled the expectations of periodograms of surfaces with five different spectral exponents at frequencies corresponding to the case of no zero-padding (Figure 3).[3] These curves may be compared to the exact spectra in Figure 4.[4] While the exact spectra vary in slope, the periodogram estimates are insensitive to the slope for several values of β. Fitting power-law functions to the linear portions of these estimate expectations ($f_\Delta < 0.2$), we see (Table I) that the estimated spectral exponent $\hat{\beta}$ clusters near 2.0 for $2 < \beta < 3$.[5] These values of β correspond to fractal dimensions that are typical for natural terrains (1.0–1.5 for profiles, 2.0–2.5 for surfaces).

Slope insensitivity is not a problem with $\hat{P}_{HAN}(f_\Delta)$, whose expected value is shown for various β in Fig. 5. The expected values of these estimates closely approximate the exact values for frequencies at which the main lobe and first two sidelobes do not overlap the low-frequency peak ($f_\Delta > 0.015625$). (Power-law fits to the upper regions of these estimates are listed in Table I). While $\hat{P}_{HAN}$ has a mean value that closely approximates the exact spectrum, this estimator suffers from a deficiency that is common to Fourier-based estimators: undesirably high variance. We examine the variance of $\hat{P}_{HAN}(f_\Delta)$ in a later section.[6]

TABLE I
POWER-LAW PARAMETERS DERIVED FROM FITS TO THE EXPECTATIONS OF PERIODOGRAM ($1/N \le f_\Delta < 0.2$), MODIFIED PERIODOGRAM ($4/N < f_\Delta \le 0.5$), PREWHITENED ($1/N < f_\Delta < 0.2$), AND CAPON'S ($1/(2p) \le f_\Delta \le 0.5$) ESTIMATORS

Theoretical	$E[\hat{P}_{PER}]$	$E[\hat{P}_{HAN}]$	$E[\hat{P}_{PW}]$	$E[\hat{P}_{CAP}]$
$c_\Delta = 1.0 \cdot 10^{-6}$	$\hat{c}_\Delta = 9.71 \cdot 10^{-7}$	$\hat{c}_\Delta = 9.99 \cdot 10^{-7}$	$\hat{c}_\Delta = 8.42 \cdot 10^{-7}$	$\hat{c}_\Delta = 1.01 \cdot 10^{-6}$
$\beta = 1.2$	$\hat{\beta} = 1.231$	$\hat{\beta} = 1.201$	$\hat{\beta} = 1.255$	$\hat{\beta} = 1.198$
$c_\Delta = 1.0 \cdot 10^{-6}$	$\hat{c}_\Delta = 1.04 \cdot 10^{-6}$	$\hat{c}_\Delta = 9.99 \cdot 10^{-7}$	$\hat{c}_\Delta = 8.63 \cdot 10^{-7}$	$\hat{c}_\Delta = 1.01 \cdot 10^{-6}$
$\beta = 1.6$	$\hat{\beta} = 1.656$	$\hat{\beta} = 1.601$	$\hat{\beta} = 1.643$	$\hat{\beta} = 1.598$
$c_\Delta = 1.0 \cdot 10^{-6}$	$\hat{c}_\Delta = 2.10 \cdot 10^{-6}$	$\hat{c}_\Delta = 9.96 \cdot 10^{-7}$	$\hat{c}_\Delta = 8.66 \cdot 10^{-7}$	$\hat{c}_\Delta = 1.02 \cdot 10^{-6}$
$\beta = 2.0$	$\hat{\beta} = 1.982$	$\hat{\beta} = 2.001$	$\hat{\beta} = 2.042$	$\hat{\beta} = 1.998$
$c_\Delta = 1.0 \cdot 10^{-6}$	$\hat{c}_\Delta = 1.87 \cdot 10^{-5}$	$\hat{c}_\Delta = 9.98 \cdot 10^{-7}$	$\hat{c}_\Delta = 8.65 \cdot 10^{-7}$	$\hat{c}_\Delta = 1.02 \cdot 10^{-6}$
$\beta = 2.4$	$\hat{\beta} = 2.032$	$\hat{\beta} = 2.402$	$\hat{\beta} = 2.443$	$\hat{\beta} = 2.397$
$c_\Delta = 1.0 \cdot 10^{-6}$	$\hat{c}_\Delta = 3.83 \cdot 10^{-4}$	$\hat{c}_\Delta = 9.96 \cdot 10^{-7}$	$\hat{c}_\Delta = 8.43 \cdot 10^{-7}$	$\hat{c}_\Delta = 1.02 \cdot 10^{-6}$
$\beta = 2.8$	$\hat{\beta} = 1.986$	$\hat{\beta} = 2.804$	$\hat{\beta} = 2.859$	$\hat{\beta} = 2.796$

B. Prewhitening

The periodogram (Fig. 2) and, to a lesser degree, the modified periodogram (Fig. 5) suffer from spectral leakage in the power-law case, especially for spectra with $2 \le \beta \le 3$. Fox and Hayes [9] and Gilbert and Malinverno [10] avoid the leakage problem by using prewhitening procedures in which they modify the surface height

[3]We emphasize that Fig. 3 shows *expected values*, $E[\hat{P}_{PER}(f)]$, (i.e., mean values) of the periodogram estimator, calculated using (9) at frequencies corresponding to the case of no zero-padding for random profiles $Z(x)$ having power-law spectra given by (17) with five different values of β. Plots of the estimator $\hat{P}_{PER}$ itself would show wide variance and departures from linearity (similar to the estimates shown in Fig. 8) and would vary for different realizations of the random process, i.e., for different samples of a given surface.

The expected values of the estimator appear linear at the low-frequency end because we have assumed in (17) that the true surface spectrum is power-law (with linear slope) down to a frequency of $f_\Delta = 0.0001$—a frequency too low to be accurately measured by the sampled profile segment. We used this assumption because surface profiles are often too short to show very long wavelength roughness components. (This was certainly true for our field work.)

[4]The expected values of the periodogram estimator in Fig. 3 have a higher total energy level than the corresponding exact spectra in Fig. 4 due to the spectral leakage that is also responsible for the slope insensitivity. Remember that $E[\hat{P}_{PER}]$ is the convolution of the true spectrum $S_{Z\Delta}$ with the transform of a window function introduced by the finite surface sample [W_T in (9)]. If the estimator were perfect, W_T would be a delta function, and the estimate at frequency f would reflect only power in the true spectrum at that frequency. In the periodogram case, however, W_T is given by (10) (a sinc^2 function), so power from many frequencies above and below f affect $\hat{P}_{PER}(f)$. Leakage from lower frequencies is particularly significant in the power-law case.

[5]For a given single periodogram, $\hat{\beta}$ may indeed take values between 2.0 and 3.0, due to the variance of the periodogram. Long data records do not reduce this variance; the variance is independent of N (see [20, p. 422]). One may reduce the variance by segmenting the long data record as described previously, but this process will lead to the expected values shown in Fig. 3. Sampling $\hat{P}_{PER}$ at frequencies other than $f_{\Delta i} = i/N$ could lead to a variety of incorrect slopes, as can be seen in Fig. 2.

[6]We have also examined the Blackman–Tukey spectral estimator $\hat{P}_{BT}$, as described in Blackman and Tukey [22]. For processes other than white noise, the BT estimator decreases variance but increases bias as compared to the periodogram (Kay [20, p. 80]). We did not include $\hat{P}_{BT}$ in our comparison because it is even more susceptible to spectral leakage (and therefore, slope insensitivity) than $\hat{P}_{PER}$. The expected value of $\hat{P}_{BT}$ is equal to the expected value of $\hat{P}_{PER}$ convolved with another window, as derived in Kay [20, p. 98]:

$$E[\hat{P}_{BT}(f_\Delta)] = \int_{-1/2}^{1/2} W(f_\Delta - \xi) E[\hat{P}_{PER}(\xi)]\, d\xi.$$

Since the BT estimator has an expected value that is the result of the convolution of the true spectrum with *two* window functions, its value at a given frequency can be greatly corrupted by leakage from lower frequencies.

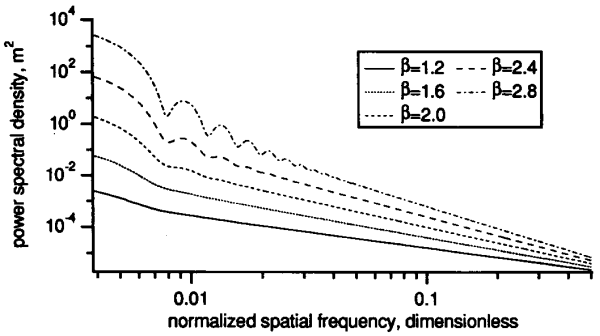

Fig. 5. Expected values of $\hat{P}_{\mathrm{HAN}}(f_\Delta)$ for five different 256-point power-law profiles. The profiles were zero-padded to 16 384 points.

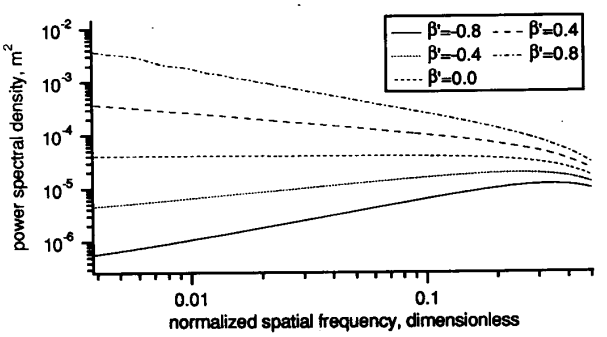

Fig. 6. Expected values of $\hat{P}_{\mathrm{PW}}(f_\Delta)$ for five different 257-point power-law profiles. The profiles were zero-padded to 16 384 points.

data to have a relatively flat spectrum, perform spectral estimation, and then correct the estimate according to the original modification.

We will examine here the simplest prewhitening approach similar to that used by Gilbert and Malinverno. If the power spectral density of the surface height is defined as [24, p. 270]

$$S_Z(f) = \lim_{T\to\infty} \frac{1}{T} E\left[\left|\int_{-T/2}^{T/2} Z(x)\exp(-j2\pi fx)\,dx\right|^2\right] \tag{18}$$

then the derivative of the surface height $dZ(x)/dx$ will have a related spectrum:

$$\begin{aligned} S_{Z'}(f) &= \lim_{T\to\infty} \frac{1}{T} E\left[\left|\int_{-T/2}^{T/2} \frac{dZ(x)}{dx}\exp(-j2\pi fx)\,dx\right|^2\right] \\ &= \lim_{T\to\infty} \frac{1}{T} E\left[\left|j2\pi f\int_{-T/2}^{T/2} Z(x)\exp(-j2\pi fx)\,dx\right|^2\right] \\ &= 4\pi^2 f^2 S_Z(f) \\ &= 4\pi^2 c\,|f|^{-\beta+2} \\ S_{Z'}(f) &= c'\,|f|^{-\beta'} \end{aligned} \tag{19}$$

and we see that the spectral exponent β' of the derivative process takes on values between -1 and 1 for $1 < \beta < 3$. The spectrum of the derivative process is more nearly flat (it is white noise for $\beta' = 0$). Since there is no pronounced peak at low frequencies, spectral leakage is less of a problem.

Gilbert and Malinverno approximate the derivative by taking first differences of the sampled data: $Z'[x_i] \approx Z[x_{i+1}] - Z[x_i]$. They then apply a Hanning window and use a periodogram to obtain a spectral estimate of $S_{Z'\Delta}(f_\Delta)$. After averaging multiple periodograms, an estimate of the spectral exponent $\hat{\beta}$ is obtained from an estimate of $\hat{\beta}'$:

$$\hat{\beta} = \hat{\beta}' + 2. \tag{20}$$

We now examine this procedure for the limited data case in which multiple periodograms are not available for averaging. We omit the Hanning window for simplicity.

We define a prewhitened spectral estimate $\hat{P}_{\mathrm{PW}}(f_\Delta)$ in terms of the first differences of the sampled data:

$$\hat{P}_{\mathrm{PW}}(f_\Delta) = \frac{1}{N}\left|\sum_{n=0}^{N-1}\{Z[x_{n+1}] - Z[x_n]\}\exp(-j2\pi f_\Delta n)\right|^2. \tag{21}$$

The expected value of the prewhitened estimator may be derived by a procedure similar to the derivation of (9):

$$E[\hat{P}_{\mathrm{PW}}(f_\Delta)] = 2\int_{-1/2}^{1/2} W_T(f_\Delta - \xi)S_{Z\Delta}(\xi)\cdot[1-\cos(2\pi\xi)]\,d\xi. \tag{22}$$

Using (22) and the modified power-law spectrum defined in (17), the expected values of the prewhitened estimator are calculated and are shown in Fig. 6. These estimates are based on 257-point profiles.

Power-law functions were fit to the linear portions of these estimate expectations ($f_\Delta < 0.2$), and the parameters $\hat{c}'$ and $\hat{\beta}'$ were converted to $\hat{c}$ and $\hat{\beta}$ using (20) and $\hat{c} = \hat{c}'/(4\pi^2)$. The results, given in Table I, show that the expected value of the spectral slope is fairly accurate because the spectral leakage has been largely eliminated. A Hanning window may still be useful in practice (since we do not know *a priori* that a spectrum is power law), but we see that leakage is not a problem for the prewhitened estimator in the power-law case. The variance of $\hat{P}_{\mathrm{PW}}(f_\Delta)$ will be examined in a later section.

C. Capon's Estimator

An alternative procedure that is more direct than the prewhitened periodogram is the use of Capon's estimator [25] (the so-called "minimum variance spectral estimator") described in Kay [20, chap. 11]. This estimator was developed originally for geological signal processing problems in which the number of sensors (and therefore the number of spatial samples) were extremely limited and posed restrictions on what could be inferred from standard spectral analysis. Capon's estimator essentially customizes a filter at each frequency of interest to minimize the total power output, subject to the constraint that the gain at the frequency of interest is unity. Therefore, the filter

may be asymmetric in sidelobe level according to the shape of the signal spectrum; in the power-law case, the sidelobes are adjusted to reduce the leakage from low-frequency components.

Capon's estimator $\hat{P}_{CAP}(f_\Delta)$ is obtained by first calculating an estimate of the autocorrelation matrix $\mathbf{R}_{ZZ}$, whose elements are defined as

$$[\mathbf{R}_{ZZ}]_{ij} = E[Z^*[n]Z[n + i - j]]. \quad (23)$$

We can estimate the elements of the autocorrelation matrix using the modified covariance method, described in [20]:

$$[\hat{\mathbf{R}}_{ZZ}]_{ij} = \frac{1}{2(N-p)}\left[\sum_{n=p}^{N-1} Z[n-i]Z[n-j] + \sum_{n=0}^{N-1-p} Z[n+i]Z[n+j]\right]. \quad (24)$$

Capon's estimator is then given by

$$\hat{P}_{CAP}(f_\Delta) = \frac{p}{\mathbf{e}^H \hat{\mathbf{R}}_{ZZ}^{-1} \mathbf{e}} \quad (25)$$

where p is the dimension of the autocorrelation matrix and

$$\mathbf{e} = [1 \quad e^{j2\pi f_\Delta} \quad e^{j4\pi f_\Delta} \quad \cdots \quad e^{j2\pi(p-1)f_\Delta}]^T. \quad (26)$$

Since (24) is an unbiased[7] and consistent estimator of the covariance matrix, we can evaluate the expected value of Capon's estimator by substituting the exact covariance matrix (obtained from the exact theoretical spectrum) into (25). This procedure was used to calculate the expected values of $\hat{P}_{CAP}(f_\Delta)$ for five values of β using a covariance matrix of dimension $p = 70$. The expected values of these estimates (Fig. 7) have good agreement with the exact spectra over a wide range of spectral slopes. Parameters of power-law functions fit to the expected values of $\hat{P}_{CAP}(f_\Delta)$ for $f_\Delta \geq 1/(2p)$ are compared with the exact spectral parameters in Table I.

The bias of Capon's estimator is independent of N because (24) is an unbiased estimator of $\hat{\mathbf{R}}_{ZZ}$. However, the bias does depend on p ($p\Delta$ is the longest lag for which the covariance is estimated). For a given data set, an increase in p will result in reduced bias at the cost of increased variance. Thus, N indirectly influences the bias because the range of p is constrained by N. We generally found $p \approx 0.3N$ to be a good compromise between variance and bias.

In the power-law case, the bias of Capon's estimator was found to increase noticeably for spatial frequencies corresponding to wavelengths much longer than $p\Delta$. We therefore discard calculated values of $\hat{P}_{CAP}(f_\Delta)$ for spatial frequencies below $1/(2p)$.

[7]Equation (24) is approximately but not strictly unbiased because all lags are not weighted equally and overlapping lags are used. A variety of covariance estimators have been examined, and (24) was found to be the preferred estimator for short data records. See Kay [20] or other texts for more information.

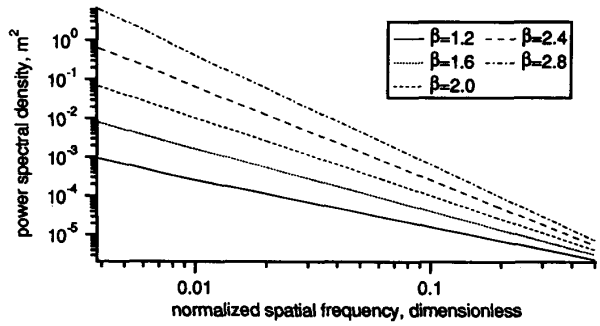

Fig. 7. Expected values of $\hat{P}_{CAP}(f_\Delta)$ for synthetic profiles with various β using an autocorrelation matrix of dimension $p = 70$. Estimates are evaluated at the same 16 384 frequencies used in Figs. 2, 5, and 6.

D. Variance Comparison

Capon's estimator, the modified periodogram with Hanning window, and the prewhitened periodogram all produce parameter estimates whose expected values closely approximate the exact values for a power-law spectrum. We now compare the estimators in terms of variance. The exact expression for the variance of the modified periodogram involves higher order moments and is usually evaluated only for a Gaussian white-noise case [21]. The statistical properties of Capon's estimator for time series data are not known [20], although some results have been derived for array data. To avoid these problems and test these estimators under actual-use conditions, we generated short synthetic topographic profiles of known statistics using a spectral synthesis algorithm. We then compare parameters obtained from Capon's, the modified periodogram, and the prewhitened periodogram estimates with those of the spectra used to create the profiles.

Our spectral synthesis algorithm closely follows [26] and consists of the following steps. 1) Generate a set of discrete Fourier amplitudes that, when squared and multiplied by $1/N$, satisfy the desired power law. While [26] used a pure power-law spectrum, we use the modified spectrum (17) to assure a zero-mean surface height. 2) Multiply the amplitudes by a Gaussian random variable such that the mean value of the amplitude satisfies the power law. 3) Generate a set of complex discrete Fourier coefficients (i.e., the FFT of a real surface) using the randomized amplitudes and a uniformly distributed random phase, enforcing symmetry conditions such that the inverse FFT will be real-valued. 4) Calculate the inverse FFT of the coefficients, resulting in a synthetic surface profile.

Using this algorithm, we generated 10 synthetic 64-point surface profiles with $\beta = 2.4$ and c_Δ, α, and σ chosen as before. We then calculated 1) Capon's estimates using a covariance matrix of dimension $p = 20$, 2) modified periodogram estimates using a full-width Hanning window, and 3) periodogram estimates based on the first differences of the surface profiles. We see in Fig. 8 that the modified periodogram and prewhitened periodogram estimates have noticeably greater variance.

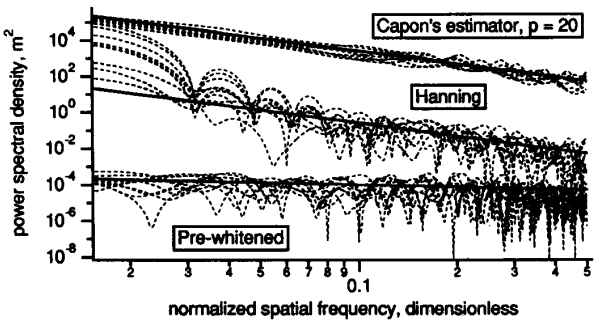

Fig. 8. Capon's, modified periodogram, and prewhitened periodogram spectral estimates for 10 different power-law profiles. The profiles were 64 points long. The modified periodogram and Capon's estimates have been offset for clarity. The solid lines represent the exact spectrum.

TABLE II
SPECTRAL STATISTICS DERIVED FROM FITS TO MODIFIED PERIODOGRAMS, PERIODOGRAMS BASED ON PREWHITENED DATA, AND CAPON'S ESTIMATORS OF TEN SYNTHETIC 64-POINT PROFILES WITH $c_\Delta = 1.0 \cdot 10^{-6}$ AND $\beta = 2.4$

Estimator	mean $\hat{c}_\Delta$	std. dev. $\hat{c}_\Delta$	mean $\hat{\beta}$	std. dev. $\hat{\beta}$
$\hat{P}_{HAN}$	$0.724 \cdot 10^{-6}$	$0.819 \cdot 10^{-6}$	2.767	0.631
$\hat{P}_{PW}$	$1.310 \cdot 10^{-6}$	$1.690 \cdot 10^{-6}$	2.469	0.567
$\hat{P}_{CAP}$	$0.891 \cdot 10^{-6}$	$0.433 \cdot 10^{-6}$	2.371	0.313

Estimation of power-law parameters from the spectral estimates is an independent problem. In this analysis, we estimate c and β by performing a minimum absolute deviation fit of a power-law function to the estimated values of the power density spectrum. The minimum absolute deviation fit, which is performed in log–log space, is more robust than a least-squares fit. To make the power-law fit independent of the frequency sampling of the spectral estimates, we evaluated the estimates at frequencies spaced very closely together so that the estimator would be a smooth curve between the sampled points. While it may be possible to design a parameter estimate based on fewer samples of the spectral estimate, such a method would require additional assumptions in the spectral model which are outside the scope of this study.

Values of the spectral estimates outside their regions of high accuracy ($4/N < f_\Delta \le 0.5$ for $\hat{P}_{HAN}$, $1/N < f_\Delta < 0.2$ for $\hat{P}_{PW}$, and $1/(2p) \le f_\Delta \le 0.5$ for $\hat{P}_{CAP}$) were discarded as before. The mean and standard deviation of the estimated roughness amplitude $\hat{c}_\Delta$ and spectral slope $\hat{\beta}$ are given in Table II. We see that the spectral parameters predicted using Capon's estimator have roughly half the variance of estimates derived from either the modified periodogram with the Hanning window or the periodogram based on prewhitened data. We therefore select Capon's estimator as the preferred estimation algorithm for use with short data records in the power-law spectrum case.

E. Formulas for Real Frequency

Expressions for the spectral estimators listed in the preceding sections were given as functions of the normalized frequency f_Δ that is dependent on the sampling interval of a measured surface profile. In remote sensing studies, estimates of the surface spectrum in terms of real spatial frequency f (in meters^{-1}) are necessary so that 1) surface features may be compared to the electromagnetic wavelength and 2) spectral estimates derived from profiles with different sampling intervals Δ may be compared or combined into a composite spectrum.

The following expressions correspond to (4), (9), (10), (6), (12), (13), (14), (15), (16), (21), (22), (25), and (26), respectively, for the case of real (nonnormalized) frequency f, where f satisfies $-1/(2\Delta) \le f \le 1/(2\Delta)$:

$$\hat{P}_{PER}(f) = \frac{\Delta}{N}\left|\sum_{n=0}^{N-1} Z[x_n] \exp(-j2\pi f\Delta n)\right|^2 \tag{27}$$

$$E[\hat{P}_{PER}(f)] = \Delta \int_{-1/2\Delta}^{1/2\Delta} W_T(f-\xi) S_Z(\xi)\, d\xi \tag{28}$$

$$W_T(f) = \frac{1}{N}\left(\frac{\sin \pi f\Delta N}{\sin \pi f\Delta}\right)^2 \tag{29}$$

$$\hat{P}_{HAN}(f) = \frac{\Delta}{NU}\left|\sum_{n=0}^{N-1} Z[x_n] w_H[n] \exp(-j2\pi f\Delta n)\right|^2 \tag{30}$$

$$E[\hat{P}_{HAN}(f)] = \Delta \int_{-1/2\Delta}^{1/2\Delta} W_H(f-\xi) S_Z(\xi)\, d\xi \tag{31}$$

$$W_H(f) = \frac{1}{4NU}\left(b_1 + \frac{1}{2}b_2 + \frac{1}{2}b_3\right)^2 \tag{32}$$

$$b_1 = \frac{\sin(\pi f\Delta N)}{\sin(\pi f\Delta)} \tag{33}$$

$$b_2 = \frac{\sin\left\{\pi\left[f - \frac{1}{(N-1)\Delta}\right]\Delta N\right\}}{\sin\left\{\pi\left[f - \frac{1}{(N-1)\Delta}\right]\Delta\right\}} \tag{34}$$

$$b_3 = \frac{\sin\left\{\pi\left[f + \frac{1}{(N-1)\Delta}\right]\Delta N\right\}}{\sin\left\{\pi\left[f + \frac{1}{(N-1)\Delta}\right]\Delta\right\}} \tag{35}$$

$$\hat{P}_{PW}(f) = \frac{\Delta}{N}\left|\sum_{n=0}^{N-1}\left\{\frac{Z[x_{n+1}] - Z[x_n]}{\Delta}\right\} \cdot \exp(-j2\pi f\Delta n)\right|^2 \tag{36}$$

$$E[\hat{P}_{PW}(f)] = 2\Delta \int_{-1/2\Delta}^{1/2\Delta} W_T(f-\xi) S_Z(\xi) \cdot [1 - \cos(2\pi\xi)]\, d\xi \tag{37}$$

$$\hat{P}_{CAP}(f) = \frac{p\Delta}{\mathbf{e}^H \hat{\mathbf{R}}_{ZZ}^{-1} \mathbf{e}} \tag{38}$$

$$\mathbf{e} = [1 \quad e^{j2\pi f\Delta} \quad e^{j4\pi f\Delta} \quad \cdots \quad e^{j2\pi(p-1)f\Delta}]^T. \tag{39}$$

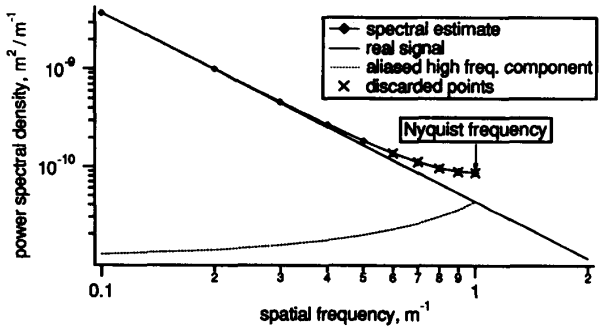

Fig. 9. Aliasing in the power-law spectrum case. Points marked (×) are discarded to reduce errors due to aliasing.

F. Aliasing

The estimates presented in the previous sections assumed that aliasing was not present, and the synthetic surface profiles were constructed to be bandlimited; i.e., they had no spatial frequency components above the Nyquist frequency $f_c = 1/(2\Delta)$. Real surfaces will generally have frequency components at spatial frequencies above f_c. As a result of a necessarily insufficient sampling rate, power at frequencies higher than f_c will be aliased into the range $-f_c \le f \le f_c$. We can derive an equation showing this result in terms of real frequency by extending the derivation of Oppenheim and Schafer [23, pp. 26–28], obtaining

$$S_{Z_{\text{aliased}}}(f) = \sum_{n=-\infty}^{\infty} S_Z\left(f + \frac{n}{\Delta}\right). \tag{40}$$

In the power-law case, the power spectral density falls off quickly with increasing frequency. The $n = 0$ (exact) and $n = 1$ (first alias) terms and their sum are plotted for a sample power-law case in Fig. 9. We see that the effects of aliasing are most significant at the high-frequency end of the spectral estimate. As a first-order correction to avoid the aliasing problem, we discard values of the spectral estimate computed for frequencies greater than $f_c/2$, as indicated in the figure.

G. Applicability to Real Data

Real geological data possess a variety of irregularities and surface statistics. Spectra of natural topography clearly cannot conform to a power-law model at all spatial frequencies—roughness features on the scale of millions of meters are unphysical, as are those at subatomic scales. However, in the studies cited in Section I as well as in our own investigations, measured spectra of topography are well modeled by a power-law spectrum in the form of (1) over some range of spatial frequencies. We have based our comparison of spectral estimators on an idealized spectrum with constant slope (except for the very-low-frequency roll-off introduced in (17) to avoid an unphysical singularity) in order to have an easy reference for comparison. Because both the Fourier estimators with windowing and Capon's estimator are local-neighborhood estimators, our comparison also illustrates the relative performance of these estimators for spectra that have variations in slope with frequency or local perturbations in level that violate monotonicity.

III. Estimation of Two-Dimensional Spectra

While the previous techniques allow the estimation of the spectrum of a linear profile, we would in general prefer a two-dimensional spectrum of surface topography. Such a spectrum might show hidden anisotropy or may indicate that the surface is isotropic in the statistical sense. In either case, the full 2-D spectrum provides valuable additional information.

Two-dimensional spectral analyses are precluded when 2-D data are not available. Spectral studies of seafloor morphology, for example, usually utilize profiles collected by bathymetric instruments that are towed by a ship, producing a seafloor profile along the ship's path. Some directional insight can be obtained by obtaining profiles in orthogonal directions.

On land, 2-D data are somewhat more accessible. Huang and Turcotte [1], [4] and England [5] use digital elevation models to estimate surface spectra, but their methods average over azimuth angle in the spectral domain. Two-dimensional data at scales of centimeters to tens of meters can be tedious and costly to obtain, necessitating smaller dimensions of a sampling grid, i.e., fewer than 100 × 100 measured points per 2-D profile.

A. Estimator Selection

Two-dimensional Fourier-based spectral estimators such as the 2-D periodogram suffer from the same problems as the corresponding 1-D estimators: leakage in the power-law case and high variance. A 2-D Capon's estimator is one solution to these problems. The 1-D Capon's estimator is readily extended to the two-dimensional case [20, sect. 15.8], at the cost of increased complexity. Inversion of the covariance matrix may become problematic because the matrix is now of dimensions $p^2 \times p^2$ rather than $p \times p$. For a similar level of resolution, the 2-D Capon's estimator will require a much greater volume of data (as will the other 2-D estimators). If such high quantities of data are not available, as is often the case for 2-D data sets, the variance of the Capon's estimate will be correspondingly higher.

B. Two-Dimensional Spectral Estimation of Isotropic Surfaces

If a surface area is known to have or can be assumed to have isotropic statistics (from knowledge of the origin of the surface, or perhaps from measured 1-D spectra in several directions), then an estimate of the 2-D roughness spectrum can be obtained from estimates of the 1-D spectrum. These 1-D spectral estimates may be obtained from individual rows of the 2-D surface height grid; we can calculate a spectral estimate for several or all rows and then average the estimates together. The resulting esti-

mate will have a variance that is much lower than that of a single row estimate in spite of the fact that the grid rows are not completely independent.

Suppose that an isotropic surface has a 2-D power spectral density $S_Z(f_x, f_y)$ that has the form of a power law down to some low spatial frequency f_{low} and some unspecified finite form below that:

$$S_Z(f_x, f_y) = S_Z(f_r) = \begin{cases} af_r^{-\gamma} & f_r \geq f_{low} \\ \text{finite} & f_r \leq f_{low} \end{cases} \quad (41)$$

where the radial spatial frequency $f_r = (f_x^2 + f_y^2)^{1/2}$. We now need to relate the parameters a and γ to the parameters of the 1-D spectrum of surface heights measured along a straight line on the same surface. This 1-D spectrum will also have the form of a power law for $f \geq f_{low}$ and can therefore be described by the parameters c and β.

To obtain this relation, we begin with the general expression for the Wiener–Khintchine relation in terms of the Fourier transform and write the correlation $E[Z(x, y)Z(x + \delta_x, y + \delta_y)]$ as $R_Z(\delta_x, \delta_y)$:

$$R_Z(\delta_x, \delta_y) = \int_{-\infty}^{\infty} \int_{-\infty}^{\infty} S_Z(f_x, f_y) \cdot \exp(j2\pi[f_x\delta_x + f_y\delta_y])\, df_x\, df_y. \quad (42)$$

Changing to radial coordinates ($\delta_x = \delta_r \cos\delta_\theta$, $\delta_y = \delta_r \sin\delta_\theta$) and noting that $S_Z(f_r, f_\theta)$ is independent of f_θ, we obtain

$$R_Z(\delta_r, \delta_\theta) = \int_0^{\infty} S_Z(f_r) f_r \int_0^{2\pi} \exp(j2\pi f_r \delta_r \cos\zeta)\, d\zeta\, df_r \quad (43)$$

where $\zeta = f_\theta - \delta_\theta$, leading to

$$R_Z(\delta_r) = 2\pi \int_0^{\infty} S_Z(f_r) J_0(2\pi f_r \delta_r) f_r\, df_r \quad (44)$$

where J_0 is the zero-order Bessel function. This expression differs from a similar (but incorrect) expression given by Voss [17, eq. (1.52)].

The 1-D and 2-D roughness spectra of an isotropic random field are related by an Abel transform [2]. This relation is more easily visualized using the surface autocorrelation functions (the inverse Fourier transforms of the 1-D and 2-D surface spectra). The 1-D autocorrelation function is a slice of the 2-D autocorrelation function:

$$S_{Z1D}(f_x) = \int_{-\infty}^{\infty} \int_{-\infty}^{\infty} R_Z(\delta_x, \delta_y)\delta(\delta_y) \cdot \exp(-j2\pi[f_x\delta_x + f_y\delta_y])\, d\delta_x\, d\delta_y. \quad (45)$$

Using Fourier transform properties:

$$S_{Z1D}(f_x) = S_Z(f_x, f_y) * \delta(f_x) = \int_{-\infty}^{\infty} S_Z(f_x, f_y')\, df_y'. \quad (46)$$

Let $S_{Z1D}(f_x, f_y)$ be given by (41), and let f_x be restricted to the power-law region, i.e., $f_x \geq f_{low}$:

$$S_{Z1D}(f_x) = 2a \int_0^{\infty} [(f_x)^2 + (f_y')^2]^{-\gamma/2}\, df_y'. \quad (47)$$

Changing variables, we have

$$S_{Z1D}(f_x) = 2a \int_{f_x}^{\infty} f_r^{-\gamma} \frac{f_r}{\sqrt{f_r^2 - f_x^2}}\, df_r \quad (48)$$

which can be integrated analytically [27, p. 201]:

$$S_{Z1D}(f_x) = \frac{a\sqrt{\pi}\,\Gamma\left(\frac{\gamma - 1}{2}\right)}{\Gamma(\gamma/2)} |f_x|^{-(\gamma - 1)} \quad (49)$$

where $\Gamma(x)$ is the gamma function.

Therefore, if $S_{Z1D}(f_x) = cf_x^{-\beta}$ for $f_x \geq f_{low}$, the 1-D and 2-D spectral parameters are related by

$$\gamma = \beta + 1 \quad (50)$$

$$a = \frac{\Gamma(\gamma/2)}{\sqrt{\pi}\,\Gamma\left(\frac{\gamma - 1}{2}\right)} c. \quad (51)$$

Equation (50) agrees with the result derived by Voss; he does not give an expression comparable to (51).

As previously discussed, 1-D profiles of a fractal surface with $1 < D_f < 2$ have power-law spectra with exponent β given by $\beta = 5 - 2D_f$, so that $3 > \beta > 1$. From (50), the 2-D power-law exponent γ satisfies $4 > \gamma > 2$, corresponding to 2-D surfaces with $2 < D_f < 3$, where $D_f = (8 - \gamma)/2$.

We next investigate the performance of the linear, averaged Capon's estimator in the determination of the 2-D power-law parameters a and γ. A variation of the 2-D spectral synthesis algorithm described by [26] was used to generate 2048 × 2048-point synthetic topographic surfaces with spectral exponents of 3.0, 3.4, and 3.6 with sampling intervals Δ of 1 cm. The exact surface spectrum was modeled as isotropic, with a form similar to (17):

$$S_Z(f_r) = \begin{cases} (\alpha/\sigma^2)|f_r| \exp(-f_r^2/[2\sigma^2]) & f_r \leq f_{low} \\ af_r^{-\gamma} & f_{low} \leq f_r \leq f_c \\ 0 & f_r \geq f_c \end{cases} \quad (52)$$

where f_r is the radial spatial frequency, $a = 2.384 \cdot 10^{-11}$, $f_{low} = 0.01\ \text{m}^{-1}$, and α and σ are chosen as before. The cut-off frequency $f_c = 1/2\Delta$ is equal to the Nyquist frequency along the f_x and f_y axes.

As noted previously, arrays of data containing over a million points are often unavailable. In practice, *in situ* surface height measurements may yield data sets that are much smaller, say, 40 × 40 points. Since such a data set is useful over a relatively narrow band of frequencies, several sparse grids may be collected at different scales,

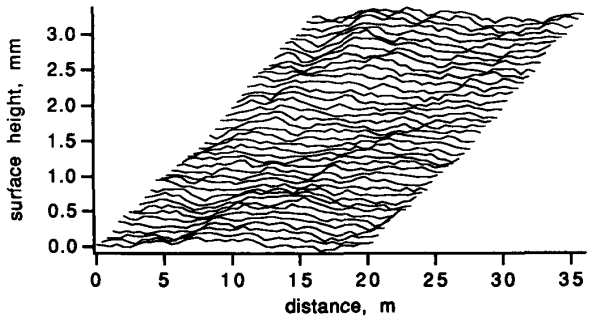

Fig. 10. 41 × 41-point sample of a 2048 × 2048-point synthetic power-law surface with $a = 2.384 \cdot 10^{-11}$ and $\gamma = 3.0$. The sampling interval is 50 cm.

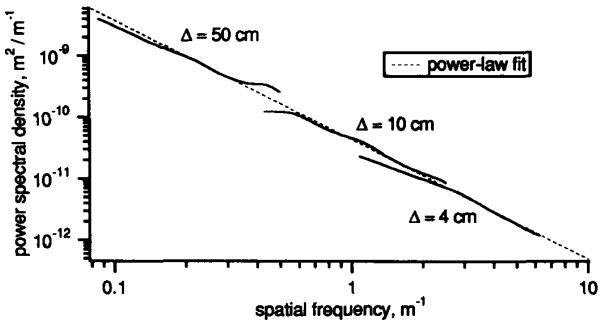

Fig. 11. Averaged Capon's estimates from 2-D synthetic surface height data at three scales with power-law fit.

TABLE III
POWER-LAW PARAMETERS DERIVED FROM FITS TO AVERAGED CAPON'S ESTIMATES AT THREE SCALES

Surface (exact)		Estimated parameters			
a	γ	mean $\hat{a}$	std. dev. $\hat{a}$	mean $\hat{\gamma}$	std. dev. $\hat{\gamma}$
$2.384 \cdot 10^{-11}$	3.0	$2.34 \cdot 10^{-11}$	$2.83 \cdot 10^{-12}$	2.971	0.041
$2.384 \cdot 10^{-11}$	3.4	$2.28 \cdot 10^{-11}$	$1.55 \cdot 10^{-12}$	3.386	0.041
$2.384 \cdot 10^{-11}$	3.6	$2.17 \cdot 10^{-11}$	$1.14 \cdot 10^{-12}$	3.555	0.061

a spectral estimate calculated for each, and a function fit to the composite of the individual spectra. Scale factors are particularly important in the calculation of these multiscale spectra.

In our investigation, we sample each 2048 × 2048-point synthetic surface at sampling intervals of 50, 10, and 4 cm, obtaining three 41 × 41-point data grids. (A sample data grid is shown in Fig. 10.) At each scale, a 1-D Capon's estimate (with $p = 12$) is calculated for each grid row at frequencies $1/(2p\Delta) < f < 1/(4\Delta)$, and the estimates are averaged over the rows. A power-law function is then fit to the averaged spectral estimates at the three scales. (A sample fit is shown in Fig. 11.) The upper frequency limit of $1/(4\Delta)$ was chosen to reduce the effect of aliasing. Estimates of 1-D power-law parameters c and β are then converted into estimates of a and γ using (50) and (51).

This process was performed on 10 synthetic surfaces at each of three spectral exponents. The mean and standard deviation of $\hat{a}$ and $\hat{\gamma}$ are listed in Table III.

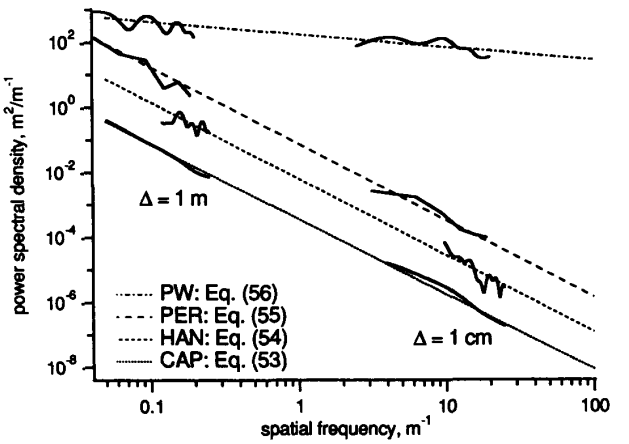

Fig. 12. Spectral estimates calculated with (from bottom to top) $\hat{P}_{CAP}$, $\hat{P}_{HAN}$, $\hat{P}_{PER}$ (with no zero-padding), and $\hat{P}_{PW}$ from surface profiles of a debris flow near Johnston Ridge at Mount St. Helens. (Spectral estimates derived from techniques other than Capon's estimator have been offset for clarity.) The dashed lines are power-law fits to the estimates; the equations of these fits are (53), (54), (55), and (56), respectively. (This and the other measured spectra from Mount St. Helens debris flows are presented in [28].).

C. Application to Measured Data

Surface roughness measurements were performed on several debris flows near Mount St. Helens in support of a study of electromagnetic scattering by volcanic terrains. The surface profiles, which were collected using several different sampling rates and profile lengths, were used to obtain estimates of the roughness spectra of the measured debris flows using the techniques described in the present report. The resulting spectra are reported elsewhere [28]. One of the spectral fits calculated from measurements of a primary debris flow near Johnston Ridge is shown in Fig. 12. This composite spectrum was derived from two surface profile grids, one with $\Delta = 1$ m, the other with $\Delta = 1$ cm. The equation of the power-law fit to the two Capon's estimates is

$$\hat{S}_Z(f) = (3.57 \cdot 10^{-4})|f|^{-2.31}. \quad (53)$$

Spectral estimates based on $\hat{P}_{HAN}$, $\hat{P}_{PER}$ (with no zero-padding), and $\hat{P}_{PW}$ were calculated from the same data for comparison with (53) and are shown in Fig. 12. Equations of the power-law fits derived from these estimators are

$$\hat{S}_{Z,HAN}(f) = (6.28 \cdot 10^{-4})|f|^{-2.36} \quad (54)$$

$$\hat{S}_{Z,PER}(f) = (7.50 \cdot 10^{-4})|f|^{-2.36} \quad (55)$$

$$\hat{S}_{Z,PW}(f) = (4.20 \cdot 10^{-4})|f|^{-2.40}. \quad (56)$$

The spectral exponents in (53)–(56) seem acceptably similar, but this is principally due to the combination of spectral estimates at different scales into a single composite spectrum. If we fit power-law functions to spectral estimates based on the $\Delta = 1$ cm data alone, we obtain the following:

$$\hat{P}_{CAP}(f) = (1.15 \cdot 10^{-3})|f|^{-2.73} \quad (57)$$

$$\hat{P}_{\mathrm{HAN}}(f) = (3.95 \cdot 10^{-3})|f|^{-3.00} \quad (58)$$

$$\hat{P}_{\mathrm{PER}}(f) = (2.12 \cdot 10^{-4})|f|^{-1.85} \quad (59)$$

$$\hat{P}_{\mathrm{PW}}(f) = (9.92 \cdot 10^{-4})|f|^{-2.75} \quad (60)$$

The Capon's, modified periodogram with Hanning window, and prewhitened spectral estimators give spectral slopes between 2.73 and 3.0, but the periodogram (with no zero-padding) gives a significantly different slope $\beta = 1.85$, illustrating the effects of spectral leakage.

IV. Conclusions

Spectral analysis is a tool of increasing importance in the characterization of topography and other natural surfaces. Numerous studies indicate that such surfaces have power-law spectra in the form of (1) over some range of spatial frequencies. This spectral form introduces unique difficulties in the spectral estimation process.

In the present work, we have shown how leakage causes some Fourier-based estimators to yield an estimated spectral exponent of 2.0 for surface profiles having spectral exponents between 2 and 3. This may explain the number of studies reporting power-law exponents of 2.0 for natural terrains. We show how Capon's estimator may be used to avoid the leakage problem and measure the surface spectrum more accurately. We also show that Capon's estimator has reduced variance, which is useful when surface data records are short, as is often the case in remote-sensing studies.

The two-dimensional Capon's estimator may be employed to compute 2-D spectra of rough surfaces. However, two-dimensional data are often unavailable or too sparse. For surfaces that are known or can be assumed to be isotropic, we show how a linear, averaged Capon's estimator can be used to estimate the 2-D power-law parameters.

Acknowledgment

The authors wish to thank several anonymous reviewers for their helpful comments and suggestions.

References

[1] J. Huang and D. L. Turcotte, "Fractal mapping of digitized images: Application to the topography of Arizona and comparisons with synthetic images," *J. Geophys. Res.*, vol. 94, pp. 7491-7495, June 10, 1989.

[2] J. A. Goff, "Comment on 'Fractal mapping of digitized images: Application to the topography of Arizona and comparison with synthetic images,'" *J. Geophys. Res.*, vol. 95, p. 5159, Apr. 10, 1990.

[3] J. Huang and D. L. Turcotte, "Reply," *J. Geophys. Res.*, vol. 95, p. 5161, Apr. 10, 1990.

[4] —, "Fractal image analysis: Application to the topography of Oregon and synthetic images," *J. Opt. Soc. Amer.: A*, vol. 7, pp. 1124-1130, June 1990.

[5] A. W. England, "The fractal dimension of diverse topographies and the effect of spatial windowing," *Geolog. Surv. Can.*, Paper 90-4: Ground Penetrating Radar, J. A. Pilon, Ed., pp. 57-61, 1992.

[6] S. R. Brown and C. H. Scholz, "Broad bandwidth study of the topography of natural rock surfaces," *J. Geophys. Res.*, vol. 90, pp. 12 575-12 582, 1985.

[7] T. H. Bell, Jr., "Statistical features of sea-floor topography," *Deep-Sea Res.*, vol. 22, pp. 883-892, 1975.

[8] —, "Mesoscale sea floor roughness," *Deep-Sea Res.*, vol. 26A, pp. 65-76, 1979.

[9] C. G. Fox and D. E. Hayes, "Quantitative methods for analyzing the roughness of the seafloor," *Rev. Geophys.*, vol. 23, pp. 1-48, Feb. 1985.

[10] L. E. Gilbert and A. Malinverno, "A characterization of the spectral density of residual ocean floor topography," *Geophys. Res. Lett.*, vol. 15, pp. 1401-1404, Nov. 1988.

[11] A. Malinverno, "Segmentation of topographic profiles of the seafloor based on a self-affine model," *IEEE J. Ocean. Engineer.*, vol. 14, pp. 348-359, Oct. 1989.

[12] R. S. Sayles and T. R. Thomas, "Surface topography as a nonstationary random process," *Nature*, vol. 271, pp. 431-434, Feb. 2, 1978.

[13] M. V. Berry and J. H. Hannay, "Topography of random surfaces," *Nature*, vol. 273, p. 573, June 15, 1978.

[14] B. B. Mandelbrot, *The Fractal Geometry of Nature*. New York: Freeman, 1983.

[15] R. J. Adler, *The Geometry of Random Fields*. New York: Wiley, 1981.

[16] B. B. Mandelbrot and J. W. Van Ness, "Fractional Brownian motions, fractional noises, and applications," *SIAM Rev.*, vol. 10, pp. 422-437, 1968.

[17] R. F. Voss, "Fractals in nature: From characterization to simulation," in *The Science of Fractal Images*, H.-O. Peitgen and D. Saupe, Eds. New York: Springer-Verlag, 1988, pp. 21-70.

[18] S. E. Hough, "On the use of spectral methods for the determination of fractal dimension," *Geophys. Res. Lett.*, vol. 16, pp. 673-676, July 1989.

[19] W. H. Press, B. P. Flannery, S. A. Teukolsky, and W. T. Vetterling, *Numerical Recipes (FORTRAN Version)*. Cambridge: Cambridge Univ., 1989.

[20] S. M. Kay, *Modern Spectral Estimation*. Englewood Cliffs, NJ: Prentice Hall, 1988.

[21] P. D. Welch, "The use of fast Fourier transform for the estimation of power spectra: A method based on time averaging over short, modified periodograms," *IEEE Trans. Audio Electroacoust.*, vol. AU-15, pp. 70-73, June 1967.

[22] R. B. Blackman and J. W. Tukey, *The Measurement of Power Spectra from the Point of View of Communications Engineering*. New York: Dover, 1958.

[23] A. V. Oppenheim and R. W. Schafer, *Digital Signal Processing*. Englewood Cliffs, NJ: Prentice Hall, 1975.

[24] R. E. Ziemer and W. H. Tranter, *Principles of Communications: Systems, Modulation, and Noise*, 2nd ed. Boston, MA: Houghton Mifflin, 1985.

[25] J. Capon, "High-resolution frequency-wavenumber spectrum analysis," *Proc. IEEE*, vol. 57, pp. 1408-1418, Aug. 1969.

[26] D. Saupe, "Algorithms for random fractals," in *The Science of Fractal Images*, H.-O. Peitgen and D. Saupe, Eds. New York: Springer-Verlag, 1988, pp. 71-136.

[27] Bateman Manuscript Project, *Tables of Integral Transforms*, vol. 2, A. Erdélyi, Ed. New York: McGraw-Hill, 1954.

[28] R. T. Austin and A. W. England, "Multi-scale roughness spectra of Mount St. Helens debris flows," *Geophys. Res. Lett.*, vol. 20, pp. 1603-1606, Aug. 6, 1993.

Richard T. Austin (S'84) was born in Maryville, TN, on September 2, 1964. He received the B.S. degree in electrical engineering from the University of Kentucky, Lexington, in 1986 and the M.S.E. degree in electrical engineering from the University of Michigan, Ann Arbor, in 1987.

He is presently pursuing the Ph.D. degree in electrical engineering at the Radiation Laboratory at the University of Michigan. During his studies, he has held a National Science Foundation Graduate Fellowship and a Michigan Space Grant Fellowship. His research interests including scattering and emission from natural surfaces and radiometric studies of the atmosphere.

Mr. Austin is a member of Tau Beta Pi and the American Geophysical Union.

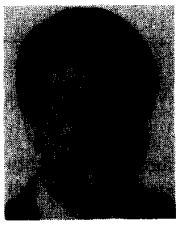

Anthony W. England (M'87-SM'89) received the B.S. degree in earth sciences (1965), the M.S. degree in geology and geophysics (1965), and the Ph.D. degree in geophysics (1970) from the Massachusetts Institute of Technology, Cambridge, MA.

His research interests have included terrestrial heat flow; geomagnetic and gravimetric studies in the northern Rockies and in Antarctica; radar studies of temperate and polar glaciers; and the microwave radiometric signatures of snow, ice, frozen and thawed soils, and planetary regoliths. He was Deputy Chief of the Office of Geochemistry and Geophysics of the U.S. Geological Survey, and was an Associate Editor for the *Journal of Geophysical Research*. He served on several federal committees concerned with Antarctic policy, nuclear waste containment, and federal science and technology. He was appointed as a NASA Scientist-Astronaut in 1967, acted as Mission Scientist for Apollo's 13 and 16, and flew as a Mission Specialist on Space Shuttle Challenger's Spacelab 2 Mission in 1985—a solar astronomy and plasma physics mission. He has been a Program Scientist for NASA's Space Station. He is currently a member of the NAS/NRC's Space Studies Board and a member of several NASA advisory committees. He has been an Adjunct Professor at William Marsh Rice University, Houston, TX, and is now a Professor of Electrical Engineering and Computer Science at the University of Michigan, Ann Arbor, MI.

Dr. England is a member of the American Geophysical Union.

Gregory H. Wakefield (S'84-M'84) received the B.A. degree *summa cum laude* in mathematics and psychology, the M.S. degree in electrical engineering, the Ph.D. degree in electrical engineering, and the Ph.D. degree in psychology, all from the University of Minnesota, Minneapolis, in 1978, 1982, 1985, and 1988, respectively.

From 1978 to 1985, he was with the Psychoacoustics Laboratory, University of Minnesota. From 1983 to 1985, he was with the Communications Laboratory and the St. Anthony Falls Hydraulics Laboratory, University of Minnesota. From 1982 to 1983, he was a consultant to the Technology Strategy Center, Honeywell, Minneapolis. From 1982 to 1985, he was consultant to the Bioscience Laboratory, Life Science Sector, 3M, St. Paul. Since 1986, he has been on the faculty of the University of Michigan, Ann Arbor, where he is currently an Associate Professor with the Department of Electrical Engineering and Computer Science. His research interests are in statistical signal processing, signal analysis and synthesis, image processing, spectral estimation, sensory systems modeling, psychoacoustics, sensory prosthetics, speech processing, and music processing. He has been involved in teaching and research in these areas and has led in the development of the educational laboratories in signal processing (SPEL) and in image processing (IPEL) at the University of Michigan.

Dr. Wakefield received the Presidential Young Investigator Award (1987), the University of Minnesota Doctoral Dissertation Fellowship (1982), and the USPHS Traineeship with the Center for Research in Human Learning (1979-1982). He is a member of Phi Beta Kappa and Sigma Xi and his professional affiliations include the Acoustical Society of America.